DISCLAIMER

This report was prepared as an account of work sponsored by an agency of the United States Government. Neither the United States Government nor any agency thereof, nor any of their employees, makes any warranty, express or implied, or assumes any legal liability or responsibility for the accuracy, completeness, or usefulness of any information, apparatus, product, or process disclosed, or represents that its use would not infringe privately owned rights. Reference herein to any specific commercial product, process, or service by trade name, trademark, manufacturer, or otherwise does not necessarily constitute or imply its endorsement, recommendation, or favoring by the United States Government or any agency thereof. The views and opinions of authors expressed herein do not necessarily state or reflect those of the United States Government or any agency thereof.

Distribution Category:
Magnetic Fusion Energy
(UC-420)

ANL/FPP/TM--220

DE88 010382

ANL/FPP/TM-220

Argonne National Laboratory
9700 S. Cass Ave.
Argonne, IL 60439

EROSION/REDEPOSITION MODELING AND CALCULATIONS FOR CARBON*

by

J. N. Brooks
Argonne National Laboratory
Argonne, IL

D. K. Brice
Sandia National Laboratory
Albuquerque, NM USA

A. B. Dewald
Georgia Institute of Technology
Atlanta, GA USA

R. T. McGrath
Sandia National Laboratory
Albuquerque, NM USA

April 1988

MASTER

*Work supported by the U.S. Department of Energy/Office of Fusion Energy

TABLE OF CONTENTS

Figures

Tables

Abstract

Several key aspects of carbon erosion/redeposition in fusion devices have been examined. These include the effects of an oblique magnetic field geometry plasma sheath on ion impingement and sputtering, and the effect of surface hydrogen buildup on sputtering. The calculations use a version of the MEASTRI hydrogen implantation code and a cloud-in-cell type sheath code. Time dependent erosion calculations have been made for the TFTR bumper limiter, using the REDEP erosion/redeposition code with updated sheath and sputtering models. The computed plasma carbon content during a TFTR limiter "deconditioning" run and for a "supershot" beam heating case is similar to measured values. The calculations predict that depletion of the near surface graphite hydrogen concentration enhances the self and hydrogen sputtering coefficients. This mechanism provides an explanation for the larger Z-effective values observed on TFTR immediately after limiter conditioning.

Introduction

Because of the importance of carbon as a fusion surface material, we have sought to improve the modeling of carbon erosion/redeposition, both to explain present day results and for future design purposes. Carbon erosion may be significantly different than that of metals in at least three respects: (1) oblique angle magnetic field geometries enhance self-sputtering more for carbon than most metals, (2) a hydrogen surface concentration reduces sputtering more, and (3) properties of redeposited carbon surface layers are less certain than for metals. Points (1) and (2) above are due primarily to the low Z (low mass) of carbon (for reasons to be explained) while (3) is due to differences in surface chemistry.

For the present work we have combined several state-of-the-art computer codes, and other relevant data, to study some of the critical issues for carbon erosion. The basic computational tool for the study is the REDEP erosion/redeposition code.[1] This has been used to analyze erosion of the TFTR carbon-coated bumper limiter. The analysis of limiter tiles removed from TFTR along with measurements of core plasma impurity content provide data which has been used to check the validity of the model.

Sheath Calculations

For most plasma surface interactions in tokamaks the magnetic field is nearly tangential to the surface. Typical field angles are $\psi = 85°$ (from the normal) for a divertor geometry (e.g. INTOR design) and $\psi \approx 89.5°$ for the TFTR bumper limiter. It has been shown that an oblique angle geometry does not appreciably change the sheath potential[2-4] but can appreciably change the incidence angles of impinging ions.[3,4] To assess the incident particle spectrum for a carbon containing plasma, with grazing magnetic field, we have made calculations using the BTHETA sheath code.[4]

For a carbon surface, the impinging plasma will contain approximately two predominant carbon charge states, C^{+6} and C^{+3}. The former results from fully stripped carbon diffusing from the core plasma while the latter results from ionization in the scrapeoff zone.[5] Sheath calculations were therefore made for a DT plasma containing C^{+3}, C^{+6} ions, in addition to He^{+2} ions. Plasma edge conditions of $Ne = 5 \times 10^{18}$ m^{-3}, $Te = Ti = 100$ eV, $B = 5T$ and $\psi = 80°$, 85° were used. Both trace impurity content ($Ni = Ne$) and finite content ($N_C = .3\ N_{DT}$) runs were made.

The angular incidence distribution for the case of $\psi = 85°$, Ne = Ni, is shown in Fig. 1 for D^+, C^{+3}, and C^{+6} ions. The T^+ and He^{+2} distributions are similar to D^+. The average values of incidence angles for $\psi = 85°$ and 80° are shown in Table 1. The results (not shown) for Ne ≠ Ni are similar.

The difference between the C^{+3} and C^{+6} spectrum, shown in Fig. 1, is due to the effect of the charge state on both the gyroradius and the electric field acceleration. To first order, a smaller gyroradius results in a more grazing ion incidence. The sheath potential for all cases run is $e\Phi \approx 3$ KTe and all ions therefore acquire an energy increment $\Delta U = N(3KTe)$ in the sheath where N is the ion charge state. It should be noted that secondary electron emission is almost completely surpressed for such highly grazing field angles[2] and so will not reduce the sheath potential.

Compared to higher Z materials, carbon ions impact at appreciably more glancing incidence. Based on previous calculations (Ref. (4) and subsequent work) W^{+4}, W^{+6} impacts at $\bar{\theta} \approx 20°$ for similar plasma conditions, while for V^{+3} ions, $\bar{\theta} \approx 30°$. Not only will carbon ions impact at more glancing incidence but carbon self-sputtering coefficients are enhanced more at such incidence, relative to higher Z materials.

For numerical reasons the sheath code was not run for $\psi > 85°$; this is planned in the future. Based on the trends shown in Table 1, impingement angles for $\psi = 89.5°$ would be even more glancing. However, the effects of surface microstructure, e.g. cone formations, could mitigate the effects of otherwise glancing impingement angles. In the present calculations for TFTR we have used the $\psi = 85°$ results.

Table 1

Average Angle of Incidence $\bar{\theta}$ (Degrees from the Surface Normal) for ions accelerated through a plasma sheath with edge plasma parameters $Ne = Ni = 5 \times 10^{18}\ m^{-3}$, $Te = Ti = 100$ eV, $B = 5T$. The magnetic field makes an angle of ψ with the surface normal.

	Average Angle of Incidence, $\bar{\theta}$	
Ion Species	$\psi = 85°$	$\psi = 80°$
D^+	66°	52°
T^+	62°	48°
He^{+2}	66°	47°
C^{+3}	51°	35°
C^{+6}	62°	40°

Surface Hydrogen Modeling

Hydrogen implantation into carbon changes the sputtering coefficients relative to pure carbon. Redeposition calculations require a reasonably fast and accurate computation of the sputtered fluxes. This is provided by the code YKI which was developed as a simplified and fast running version of the MEASTRI[6] code. The YKI code accepts as input time dependent values for D^+, C^{+6}, and C^{+3} fluxes and energies, together with their respective sputtering coefficients for pure carbon. The code follows the buildup of the surface hydrogen concentration and computes the resulting sputtering coefficients as a function of time. Here we provide a brief description of the sputtering model incorporated in YKI which is relevant for the present application.

The YKI code calculates the evolution of the near surface atomic number densities $N_K(x,t)$, which satisfy:

$$\frac{dN_K}{dt} = \begin{cases} \phi_K\, P_K(x,t), & x \geq x_o(t) \\ 0, & x < x_o(t) \end{cases} \qquad (1)$$

where Φ_K is the incident flux of K - type atoms, and $P_K dx$ is the probability that a K-type projectile implanted at time t will come to rest in the interval (x, x + dx). (The two carbon energy groups are treated as separate "species" in the calculation but are added together to obtain the final carbon sputtering flux). In equation (1) $x_o(t)$ represents the instantaneous location of the surface which is eroded by the incident particles. We point out that even when carbon atoms are implanted at a more rapid rate than lost to sputter erosion (net growth) the surface still experiences erosion since the redeposition occurs well below the surface where the implanted atoms come to rest. The erosion velocity is given by $V_o(t) = dx_o/dt$, and the sputtered flux of K-type atoms is given by $R_K(t)$, where

$$R_K(t) = V_o(t)\, N_{Ko}(t) \tag{2}$$

and $N_{Ko}(t) = N_K(x_o,t)$, the surface concentration of K-type atoms. $V_o(t)$ is determined as follows. Let $S_{J,K}$ be the sputtering coefficient for J-projectiles on an elemental target of K-type atoms, and define partial sputtered fluxes F_K by:

$$F_K(t) = \sum_J \Phi_J\, S_{J,K}\, N_{Ko}(t)/N_{To} \tag{3}$$

where

$$N_{To}(t) = \sum_i N_{io}(t) \tag{4}$$

The corresponding sputtered flux of standard atoms is then given by $F_{SDT}(t)$, where:

$$F_{STD}(t) = \sum_J \varepsilon_J F_J(t) \tag{5}$$

with $V_o(t)$ then defined in terms of the surface concentration of standard atoms by

$$F_{STD}(t) = V_o(t) \sum_J \varepsilon_J N_{Jo}(t) \tag{6}$$

From equations 3, 5, 6, V_o can be evaluated. Then equation 2 becomes

$$R_K = \frac{N_{Ko}}{\sum_J \varepsilon_J N_{Jo}(t)} \sum_{I,J} \Phi_I S_{I,J} \varepsilon_J N_{Jo}/N_{To} \tag{7}$$

where $\{\varepsilon_K\}$ is the relative stopping power of the K-type atoms. YKI uses the approximate time dependent solutions to the above equations, which are solved using the method of equivalent atomic stopping (MEAS)[7,8], along with gaussian approximations to the $\{P_K\}$. Comparison of YKI calculations with those obtained from the full MEASTRI code show agreement to within 15%, which is sufficient for our applications.

REDEP Modeling

The REDEP code[1] computes the erosion and redeposition of a limiter or divertor surface. Sputtering, plasma impurity transport, and redeposition are modeled. The code solves the integral equations for the net erosion rate by iteration and finite difference methods. The latest version of the code, REDEP7, was set up to model the 3-D TFTR bumper limiter case. Spatial features of the limiter were modeled in detail[9] using 192 spatial points per half-bay limiter segment. The sputtered neutral flux at each spatial point is computed with 10 emitted energies and 40 solid angles. The code has been used to compute metalic impurity transport as well as carbon.[9]

Sputtering models used for the TFTR carbon calculations are as follows. For deuterium sputtering (ions and charge exchange neutrals) sputtering coefficients for pure carbon are computed using the DSPUT code[10] with average angles, $\bar{\theta} = 60°$ for D^+ and $\bar{\theta} = 45°$ for D^0 and at energies determined by the plasma temperature near each limiter point. It should be noted that DSPUT predicted normal incidence yields match measured values[11] very closely. Self-sputtering coefficients for pure carbon were computed using the models of Ref. (12) and (13) for normal incidence yields and angular-enhanced yields respectively. The normal incidence self-sputtering yields were mutliplied by a factor of 0.9 so as to better match experimental data. As discussed, the pure carbon sputtering coefficients are used as input to YKI which computes the adjusted yields for hydrogen containing carbon. No chemical sputtering was assumed although this can be handled by the REDEP code if appropriate.

Edge plasma parameters, e.g., temperature and density profiles, were taken from estimates derived from TFTR D-alpha and other measurements. In general, plasma conditions during a shot are quite complicated and can only be approximately modeled at this time. For the present work all plasma parameters except for the plasma carbon concentration and the resulting carbon flux to the limiter are taken as constant in time. The carbon flux changes with time as sputtering coefficients change due to surface hydrogen accumulation.

Several other modeling issues are worth briefly noting. The sputtered energy spectrum used in REDEP for carbon is the random collision cascade model.[14] This appears to conform reasonably well to measurements, at least for normal incidence.[15] Cosine type angular emission is used; this is easily changed but data/models for non-normal incidence needs further

development. Finally, a key issue for carbon concerns the sputtering and adhesion properties of redeposited carbon. There is some data for such material, e.g. Ref. (16,17) but considerably more information is required. The present approach is to assume identical properties to the original material.

REDEP Results for TFTR

Results from the combined REDEP/MEASTRI model were obtained for TFTR discharges following limiter conditioning. Initially the active surface area of the bumper limiter, that receiving direct charged particle flux, is believed to be depleted of near surface deuterium through He conditioning.[18] The REDEP code was used to simulate a case where conditioning was followed by a series of identical ohmic discharges. The charged particle flux onto the limiter surface as a function of poloidal angle above the outboard midplane is shown in Figure 2 for a typical toroidal location. The flux varies with changing angle of incidence and with increasing distance from the last closed flux surface (plasma minor radius = 80 cm, bumper limiter minor radius = 100 cm). Also shown is the plasma temperature at the surface of the limiter. The plasma parameters have been deduced from analysis of the D_α signals on the inner bumper limiter.[19]

Using the REDEP Code, these fluxes are applied to the limiter and the time dependence of the deuterium concentration in the near surface layer calculated. Figure 3 shows the predicted time dependence of the (average) yields for self (C^{+3} + C^{+6}) and deuterium (D^+ + D^0) sputtering across the limiter surface. Near the center of the bumper limiter self-sputtering yields for carbon are very close to unity just after conditioning (t = 3.7 s). In fact, for a surface fully depleted of deuterium the predicted self-sputtering

yields are slightly in excess of unity on some portions of the limiter and the REDEP calculation is unstable. In reality, the surface is probably never completely depleted of deuterium and we begin the calculations with some D still resident in the carbon surface. As the discharges progress deuterium builds up in the near surface layers and the sputtering yields decrease as shown in Fig. 3. The spatial profiles for this buildup are shown in Fig. 4.

The local deuterium concentrations are averaged over the poloidal extent of the limiter and the averaged value as a function of plasma exposure time is shown in Fig. 5. In these calculations the near surface D inventory increases rapidly then levels off to a steady-state value of about 28% after about 30 plasma seconds. The level of saturation is consistent with RBS measurements of near surface D concentration made on tile samples removed from the machine.[20] In the REDEP calculation we also follow the C impurity concentration in the core plasma. Figure 5 also shows that the initial C concentration (N_c/N_d) in the plasma is calculated to be about 20%. On successive discharges the core plasma carbon concentration decreases reflecting the decrease in the carbon sputtering yields. The core plasma carbon concentration reaches a steady-state level of ~7% after about 25 plasma seconds (6 - four second flatop discharges). As shown in Fig. 6 this time dependence is reasonably consistent with the observed rate of change of Z-effective reported by Ramsey [21] for a deconditioning sequence of ohmic discharges. Additional work needs to be completed to determine if the deuterium recycling behavior (rate of limiter saturation) predicted by the model is consistent with the observed increases in electron density and D-alpha brightness that occur during these deconditioning sequences.

REDEP results for a neutral beam discharge following conditioning show a similar trend. The carbon concentration for this "supershot" regime is

predicted to be in excess of 20%, the exact value depending on the assumed initial D concentration. The computed concentration decreases to ~5% for a saturated carbon surface.

Discussion

Initial results from the combined REDEP/MEASTRI/BTHETA model were obtained for TFTR discharges on the carbon bumper limiter. These provide some insight into a possible mechanism for the high carbon concentrations and low hydrogen recycling coefficients following limiter conditioning. The calculations predict high carbon self-sputtering cascades due to near unity carbon self-sputtering coefficients as well as high deuterium sputtering coefficients, in hydrogen depleted carbon surface layers. A key reason for this appears to be the off normal particle incidence angles that result from an oblique magnetic field geometry. In general, data and further analysis on oblique incidence boundary conditions and redeposited carbon sputtering properties are needed for a realistic design assessment of future carbon use.

References

1. J. N. Brooks, Nucl. Tech./Fusion 4(1983) 33.
2. U. Daybeldge and B. Bein, Phys. Fluids, 24(1981) 1190.
3. R. Chodura, Phys. Fluids 25(1982) 1628.
4. A. B. Dewald, A. W. Bailey and J. N. Brooks, Phys. Fluids 30(1987) 267.
5. C. D. Boley and J. N. Brooks, FED/INTOR/ICFW182-16, Chap. VI, Georgia Inst. of Tech. (1982).
6. D. K. Brice, Proc. Eighth International Conference on Plasma Surface Interactions in Controlled Fusion Devices, J. Nuc. Mat., to be published.
7. W. R. Wampler and D. K. Brice, J. Vac. Sci. Tech. A4(1986) 1186.
8. S. T. Picraux, J. Y. Tsao, and D. K. Brice, Nucl. Inst. and Meth. B19(1987) 21.

9. R. T. McGrath and J. N. Brooks, Transport of Sputtered Impurities and Deuterium in the Vicinity of the TFTR Inner Bumper Limiter, Proc. Eighth International Conference on Plasma Surface Interactions, J. Nucl. Mat., to be published.

10. D. L. Smith, et al., Proc. 9th Symposium on Engineering Problems of Fus. Res., IEEE Pub #81CH1715-2 (1981) 719.

11. J. Roth, J. Nuc. Mat. 145-147(1987) 87.

12. N. Matsunami, et al., Atomic Data and Nuclear Tables 31(1984) 1.

13. Y. Yamamura, Y. Itikawa and N. Itoh, IPPJ-AM-26 (Inst. Plasma Phys. Nagoya University), (1983).

14. N. Thompson, Philos. Mag. 18(1968) 377.

15. P. Bogen, H. F. Isobele and and P. Merteus, J. Nucl. Mat. 145-147(1987) 434.

16. A. E. Pontau, et al., J. Vac. Sci. Tech. A4(1983) 3.

17. A. E. Pontau, R. A. Causey and J. Bohdansky, J. Nuc. Mat. 145-147(1987) 775.

18. H. F. Dylla, et al., Nuc. Fus. 8(1987) 1221.

19. D. Heifetz, et al., "H-α Studies in TFTR," ibid.

20. W. R. Wampler, et al., "Deposition of Carbon, Deuterium, and Metals on the Wall and Limiter of the Tokamak Fusion Test Reactor," Proc. 34 Natl. Symp. of the American Vac. Soc., Anaheim, CA, (1987), JVST A(1988) in press.

21 A. Ramsey, Princeton Plasma Physics Laboratory, Personal Communication, 1988.

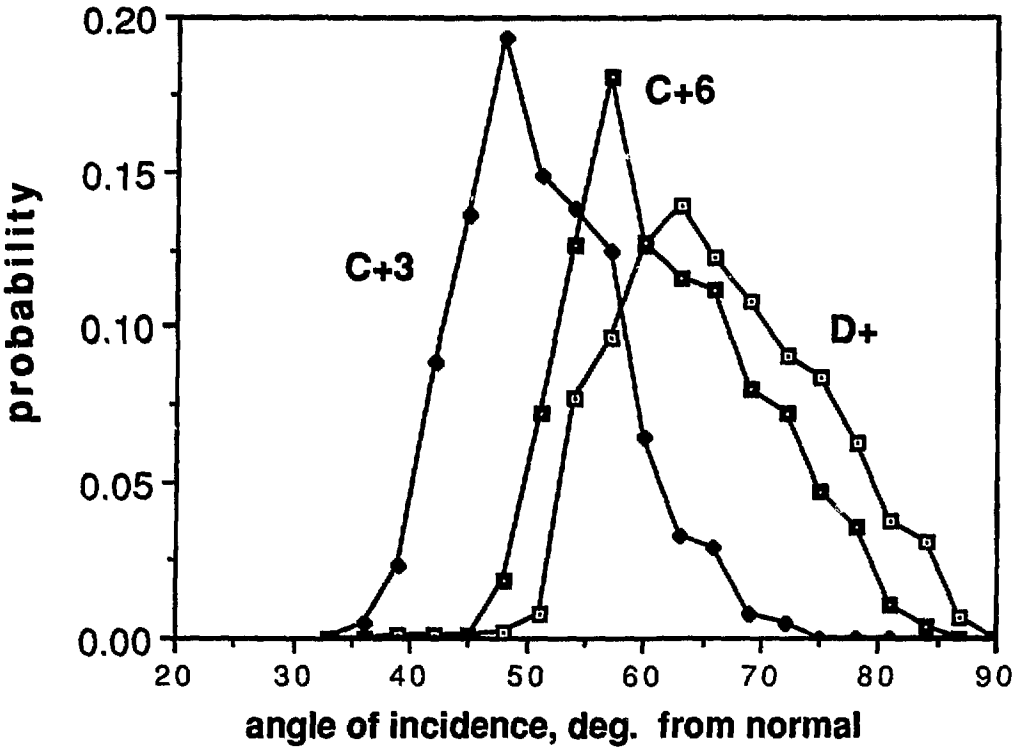

Fig. 1 Angular impingement spectrum for C^{+3}, C^{+6}, and D^{+} ions accelerated through a plasma sheath.

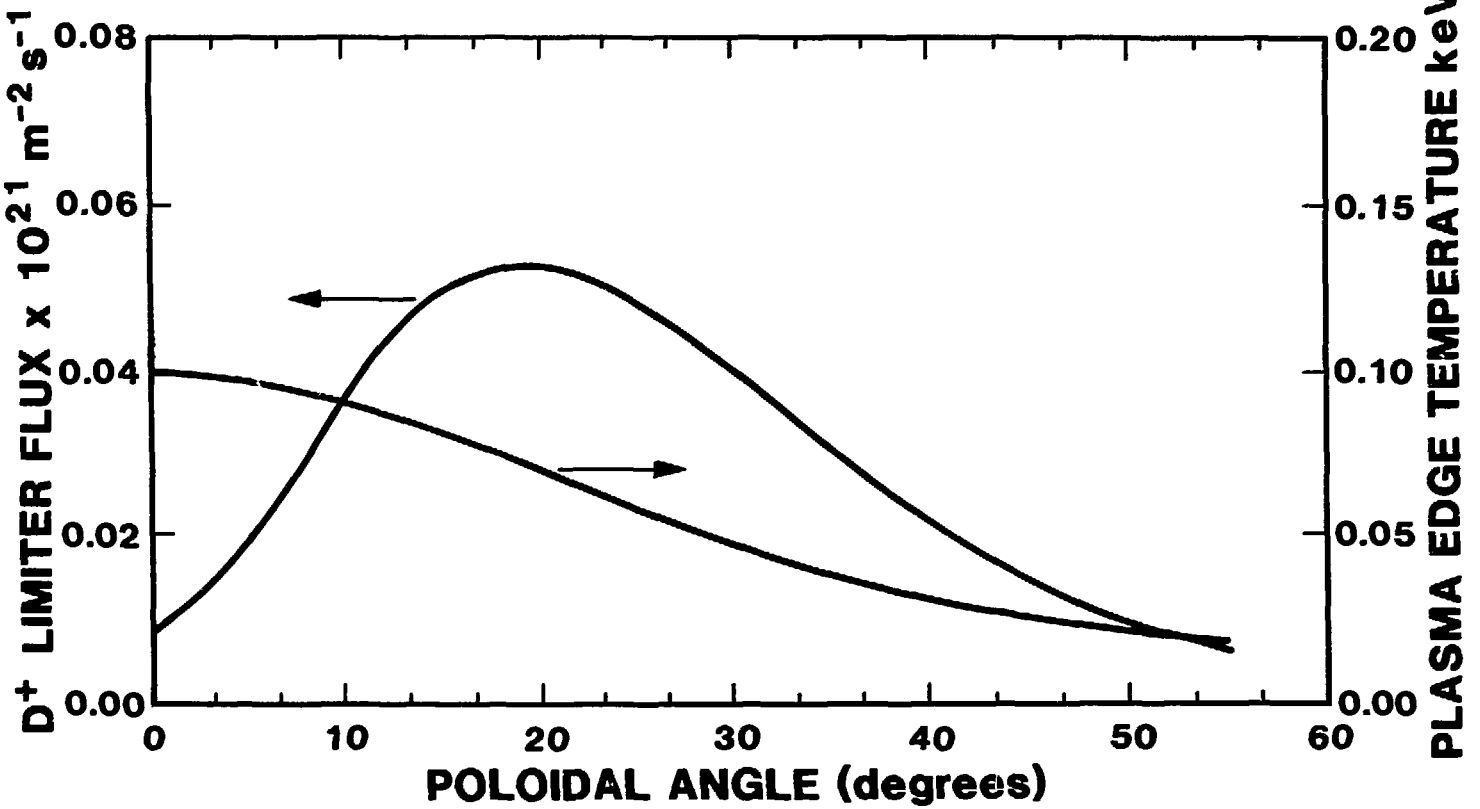

Fig. 2 Poloidal variation of incident flux and plasma temperature at the surface of the inner bumper limiter.

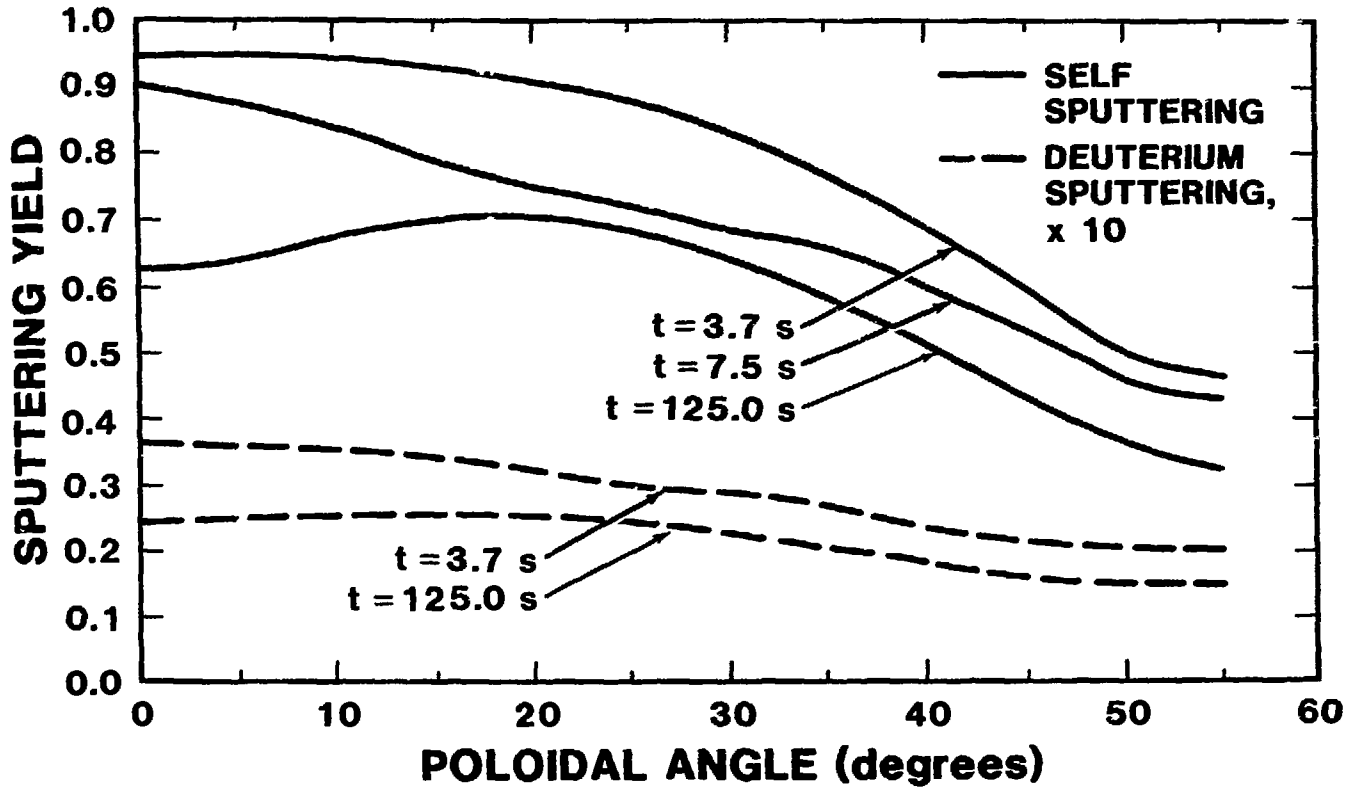

Fig. 3 Sputtering yields across the surface of the inner bumper limiter parameterized by plasma exposure time after He conditioning.

Fig. 4 Spatial profiles of D concentration in the graphite near surface layers parameterized by plasma exposure time after He conditioning.

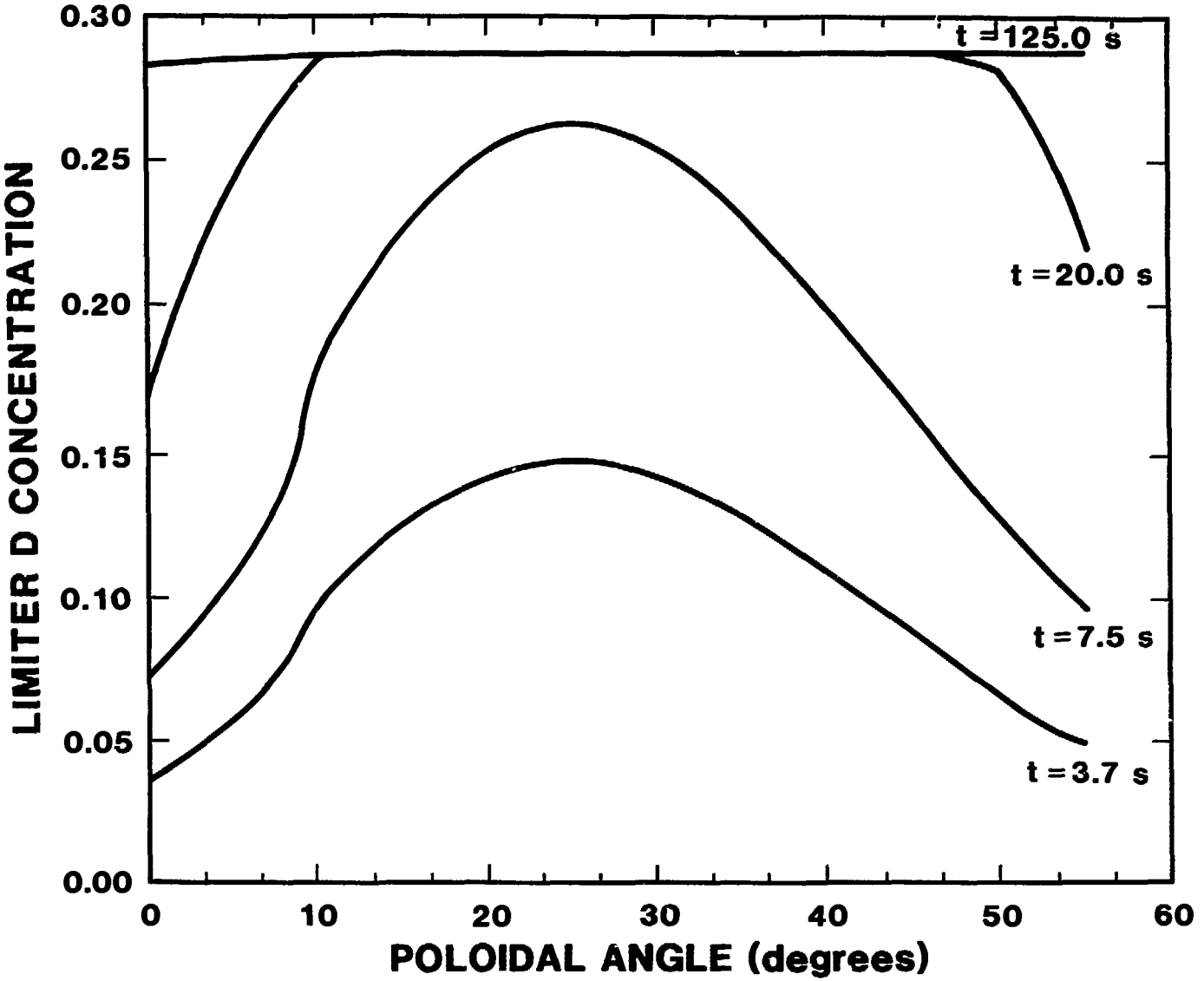

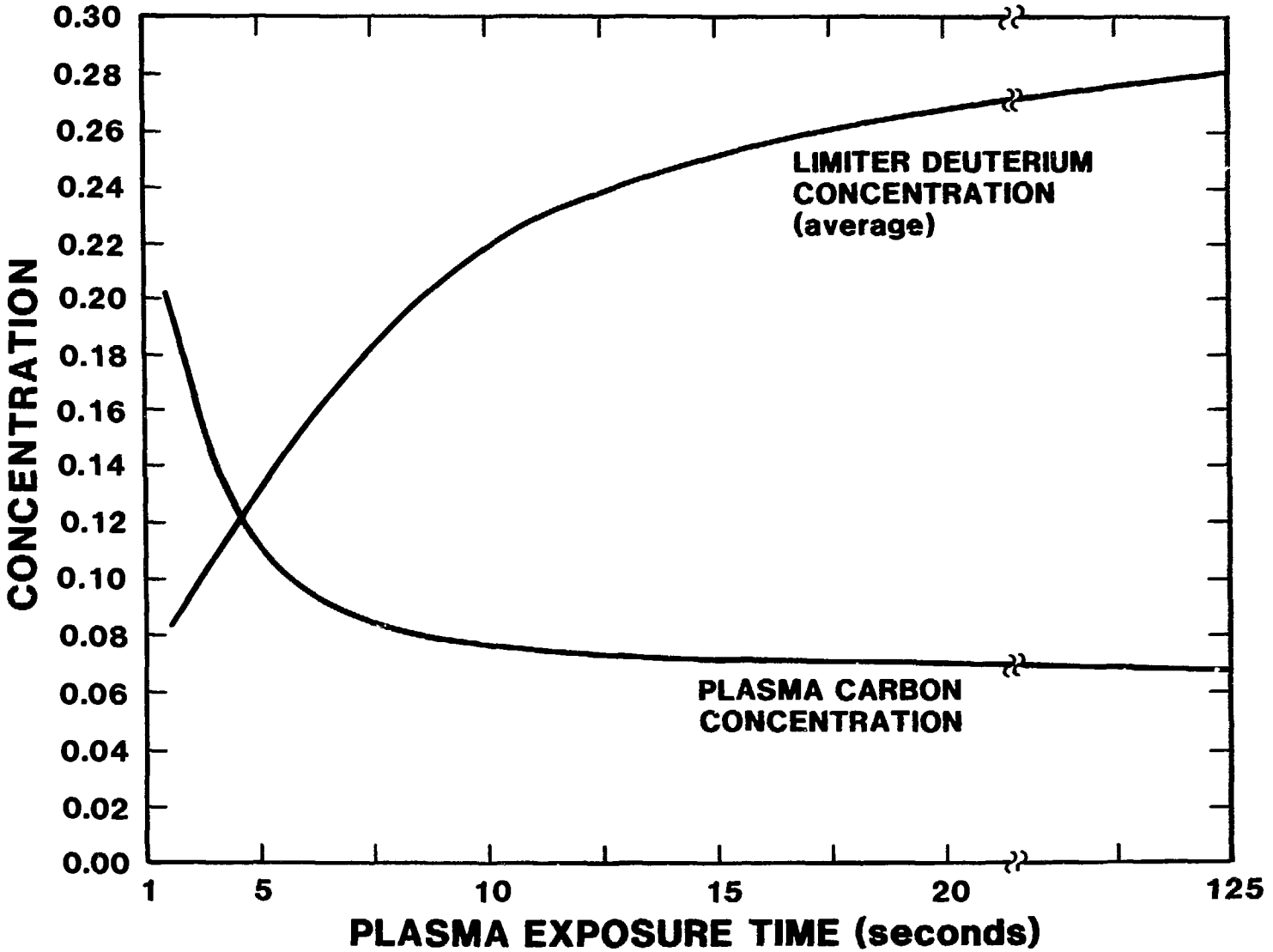

Fig. 5 Average D concentration in the near surface layers of the inner bumper and core plasma carbon concentration (n_C/n_i).

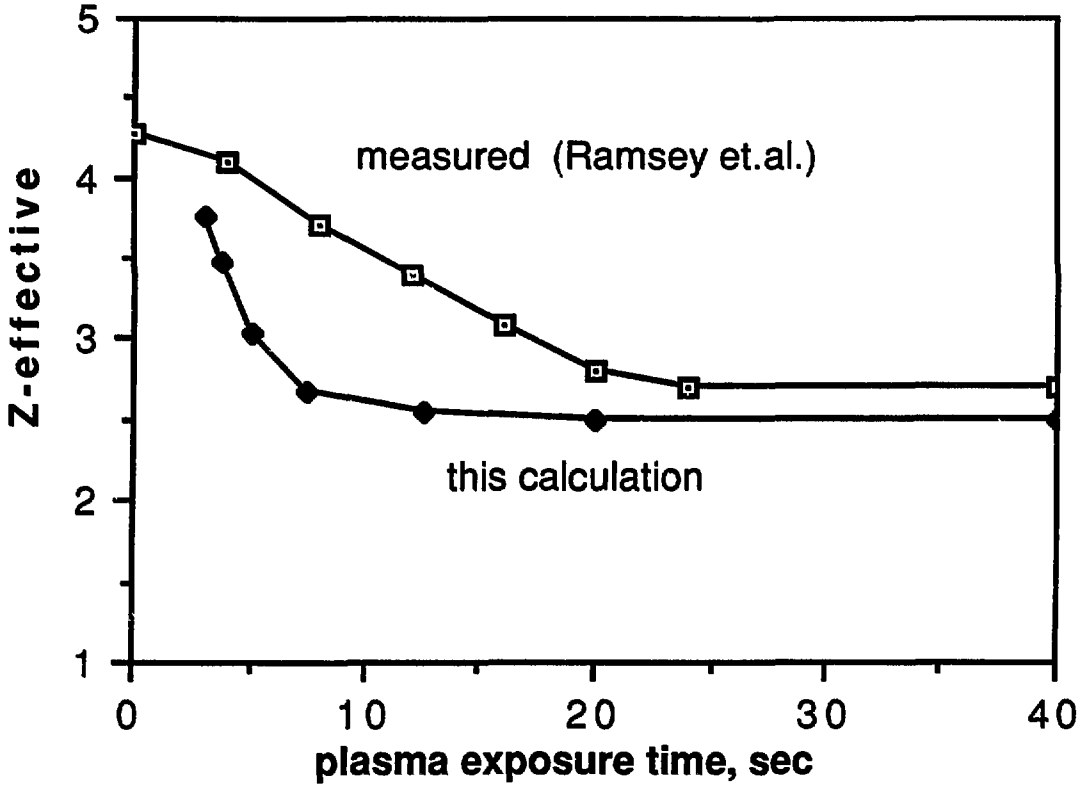

Fig. 6 Zeff from measured values and from present calculations.

DISTRIBUTION LIST FOR ANL/FPP/TM-220

Internal

C. Baker
M. Billone
J. Brooks (10)
Y. Cha
O. Chopra
R. Clemmer
D. Ehst
K. Evans
P. Finn
Y. Gohar
L. Greenwood
D. Gruen
A. Hassanein
T. Hua
C. Johnson
A. Krauss
Y. Liu
B. Loomis
S. Majumdar
R. Mattas
B. Picologlou
K. Porges
C. Reed
D. Smith
H. Stevens
D. Sze
L. Turner
T. Yule
FPP Files (25)
ANL Contract File
ANL Library
ANL Patent Dept.
TIS Files (3)

External:

DOE-TIC, for distribution per UC-420 (39)
Manager, Chicago Operations Office
R. Bastasz, Sandia National Laboratory, Livermore
D. Brice, Sandia National Laboratory, Albuquerque (3)
D. Buchenauer, Sandia National Laboratory, Livermore
R. Causey, Sandia National Laboratory, Livermore
R. Clausing, Oak Ridge National Laboratory
A. Dewald, Georgia Institute of Technology
B. Doyle, Sandia National Laboratory, Albuquerque
H. F. Dylla, Princeton Plasma Physics Laboratory
A. Ehrhardt, Princeton Plasma Physics Laboratory
R. Fleming, Princeton Plasma Physics Laboratory
A. Haasz, University of Toronto
Y. Hirooka, University of California, Los Angeles
W. Hsu, Sandia National Laboratory, Livermore
S. Kilpatrick, Princeton Plasma Physics Laboratory
P. La Marche, Princeton Plasma Physics Laboratory
W. Langer, Princeton Plasma Physics Laboratory
R. Langley, Oak Ridge National Laboratory
S. Lee, Sandia National Laboratory, Albuquerque
D. Manos, Princeton Plasma Physics Laboratory
R. McGrath, Sandia National Laboratory, Albuquerque (3)
B. Mills, Sandia National Laboratory, Livermore
R. Nygren, University of California, Los Angeles
A. Pontau, Sandia National Laboratory, Livermore
M. Ulrickson, Princeton Plasma Physics Laboratory
W. Wampler, Sandia National Laboratory, Albuquerque
J. Whitley, Sandia National Laboratory, Albuquerque
K. Wilson, Sandia National Laboratory, Livermore
K. Wright, Princeton Plasma Physics Laboratory
T. Tomabechi, Japan Atomic Energy Research Institute, JAPAN
W. Verbeeck, CEC, BELGIUM
Prof. Vetter, Kernforschungszentrum Karlsruhe und Verwaltung, WEST GERMANY
Biblicthek, Max-Planck-Institute fur Plasmaphysik, WEST GERMANY

Bibliothek, Institute fur Plasmaphysik, KFA Julich, WEST GERMANY
C.E.A. Library, Fontenay-aux-Roses, FRANCE
Librarian, Culham Laboratory, ENGLAND
Library laboratorio Gas Ionizati, ITALY
Thermonuclear Library, Japan Atomic Energy Research Institute, JAPAN